# Propagation of methane detonation in coal dust suspensions with different concentrations

Jingtai Shi[a,b], Yong Xu[b], Wanxing Ren[a], Huangwei Zhang[b]
[a] School of Safety Engineering, China University of Mining and Technology, Xuzhou, 221116, China
[b] Department of Mechanical Engineering, National University of Singapore, 9 Engineering Drive 1, Singapore 117576, Republic of Singapore

## 1 Introduction

Methane/coal dust explosion has been significant hazards in process and mining industries. However, many studies are based on experiments, in which coal dust and methane explosions are investigated independently, without due consideration of the microscopic characteristics which occur when both methane and coal dust are present as mixtures [1-3]. Coal dust is a tiny particle with a large specific surface area and strong oxidizing ability, which can absorb a large amount of energy to analyze the volatilization of coal dust particles and form a certain concentration of combustible gas around the particles while being exposed to external heat. The concentration and particle size of coal dust have a great influence on the process of methane/coal dust explosion [4]. In this study, two-dimensional methane/coal dustdetonation propagation is studied. The propagation process of gas and coal dust explosions under five different coal dust concentrations is analyzed. Moreover, general features of two-phase and detailed detonation structures are well captured. Detonation process of different coal dust concentrations are analyzed through looking into the evolutions of detonation frontal structure and detonation propagation speed. For the higher concentrations coal dust, the detonation wave first experiences decoupling of the reaction front and shock, and is then re-initiated. The results from this study are of great significance for the study of suppressing methane/coal dust mixed explosion.

## 2 Governing equation

The Eulerian-Lagrangian method is used for multi-component, reactive, two-phase, compressible flows. They are solved by a well-validated numerical solver, *RYrhoCentralFOAM* [5-10], developed from OpenFOAM 6.0. The formulations for gas phase and solid particulate phase are presented below.

### *2.1 Gas phase*

The governing equations of mass, momentum, energy, and species mass fraction are solved for the gas phase. They respectively read

$$\frac{\partial \rho}{\partial t} + \nabla \cdot [\rho \mathbf{u}] = S_{mass}, \tag{1}$$

$$\frac{\partial (\rho \mathbf{u})}{\partial t} + \nabla \cdot [\mathbf{u}(\rho \mathbf{u})] + \nabla p + \nabla \cdot \mathbf{T} = \mathbf{S}_{mom}, \tag{2}$$

$$\frac{\partial (\rho \boldsymbol{E})}{\partial t} + \nabla \cdot [\mathbf{u}(\rho \boldsymbol{E} + \boldsymbol{p})] + \nabla \cdot [\mathbf{T} \cdot \mathbf{u}] + \nabla \cdot \mathbf{j} = \dot{\omega}_T + S_{rad} + S_{energy}, \tag{3}$$

$$\frac{\partial (\rho Y_m)}{\partial t} + \nabla \cdot [\mathbf{u}(\rho Y_m)] + \nabla \cdot \mathbf{s_m} = \dot{\omega}_m + S_{species,m}, (m = 1, \dots M-1). \tag{4}$$

**Correspondence to: shijingtai@cumt.edu.cn (J. Shi), huangwei.zhang@nus.edu.sg (H. Zhang)**

In above equations, $t$ is time and $\nabla\cdot(\cdot)$ is the divergence operator. $\rho$ is the gas density, $\mathbf{u}$ is the velocity vector, and $T$ is the gas temperature. $p$ is the pressure, updated from the equation of state, i.e., $p=\rho RT$. $R$ is the specific gas constant and is calculated from $R=R_u\sum_{m=1}^{M}Y_m W_m^{-1}$. $W_m$ is the molar weight of $m$-th species and $R_u=8.314$ J/(mol·K) is the universal gas constant. The viscous stress tensor $\mathbf{T}$ in Eq. (2) is modelled by $\mathbf{T}=-2\mu[\mathbf{D}-\mathrm{tr}(\mathbf{D})\mathbf{I}/3]$. Here $\mu$ is the dynamic viscosity and follows the Sutherland's law [11]. $\mathbf{D}\equiv[\nabla\mathbf{u}+(\nabla\mathbf{u})^T]/2$ is the deformation gradient tensor. In Eq. (4), $Y_m$ is the mass fraction of $m$-th species, and $M$ is the total species number. $\mathbf{s_m}=-D_m\nabla(\rho Y_m)$ is the species mass flux, and $D_m$ is the mass diffusivity. Moreover, $\dot{\omega}_m$ is the production or consumption rate of $m$-th species by all $N$ reactions. The term $\dot{\omega}_T$ in Eq. (3) represents the combustion heat release and is estimated as $\dot{\omega}_T=-\sum_{m=1}^{M}\dot{\omega}_m\Delta h_{f,m}^o$, in which $\Delta h_{f,m}^o$ is the formation enthalpy of $m$-th species. $\boldsymbol{E}\equiv e+|\mathbf{u}|^2/2$ is the total non-chemical energy, and $\boldsymbol{e}$ is the specific sensible internal energy. $S_{rad}$ is the heat radiation term and is modelled with discrete ordinates method, through solving radiative transfer equations. The gas-solid coupling is implemented through the source terms of $S_{mass}$, $\mathbf{S}_{mom}$, $S_{energy}$ and $S_{species,m}$.

*2.2 Solid particulate phase*

The Lagrangian method is used to track the coal particles, and the equations of mass, momentum and energy are solved. The details can be found in Refs. [5,6]. For char ($C_{(s)}$) surface reactions, it is assumed to be $C_{(s)}+O_2\rightarrow CO_2$, and the kinetic/diffusion-limited rate model [12] is used. In this model, the diffusion rate coefficient $D_0$ and kinetic rate coefficient $R_k$ are respectively calculated through

$$D_0=C_1\frac{\left[(T+T_p)/2\right]^{0.75}}{d_p}, \tag{5}$$

$$R_k=C_2e^{-(E/RT_p)}. \tag{6}$$

The above two rate coefficients are weighted to derive a char combustion rate $dm_p/dt=-A_p p_{ox}D_0R_k/(D_0+R_k)$. $T_p$ is the particle temperature, $d_p$ is the particle diameter, the constants $C_1$ and $C_2$ are $5\times10^{-12}$ kg/(m·s·Pa·K$^{0.75}$) and 0.002 kg/(m$^2$·s·Pa), respectively, whilst the activation energy $E$ is $7.9\times10^7$ J/kmol [13,14], $A_p$ is the surface area of the particles, $p_{ox}$ is the partial pressure of oxidant species in the surrounding gas.

## 3 Physical model and numerical implementation

Two-dimensional methane/coal dust detonations are studied, and the schematic of physical model and computational domain is shown in Fig. 1. The length ($x$-direction) and width ($y$-direction) are 0.3 m and 0.025 m, respectively. It includes detonation development (0−0.2 m) and coal dust (0.2−0.3 m) sections, as marked in Fig. 1. The whole domain is initially filled with stoichiometric $CH_4/O_2/N_2$ (mole ratio of 1:2:1.88) mixture. The gas temperature and pressure are $T_0$ = 300 K and $P_0$ = 50 kPa, respectively. In the two-phase section, devolatilized coal dust particles are loaded to mimic the coal dust suspensions for methane/coal dust detonation. This enables us to concentrate on the effects of char combustion on methane detonation dynamics, as demonstrated in Fig. 1. The properties of coal dust particles are shown in Table 1 and the coal concentration is varied in our simulations. The upper and lower boundaries of the computational domain in Fig. 1 are periodic. For the left boundary ($x$ = 0), the wave transmissive condition in OpenFOAM is enforced for the pressure, whereas the zero-gradient condition for other quantities. For the right boundary at $x$ = 0.3 m, zero-gradient conditions are assumed. A reduced chemical mechanism (DRM 22) developed by Kazakov and Frenklach [15] is used for methane combustion, which contains 24 species and 104 reactions.

Cartesian cells are used to discretize the domain in Fig. 1 and the mesh cell size transitions from 50 μm ($x$ = 0–0.14 m) to 25 μm (0.14–0.3 m). To minimize the spatially variable resolution effects on the detonation propagation, a refined area (0.14–0.2 m) with mesh size of 25 μm is included to connect

the detonation development and coal-dust sections. The resultant total cell numbers in the simulations are 7,800,000.

Table 1. The properties of coal dust particles

| Particle diameter [μm] | Mass % | | Heat capacity [J kg$^{-1}$ K$^{-1}$] | Density [kg m$^{-3}$] |
|---|---|---|---|---|
| | Fixed carbon | Ash | | |
| 1 | 88.72 | 11.28 | 710 | 1,500 |

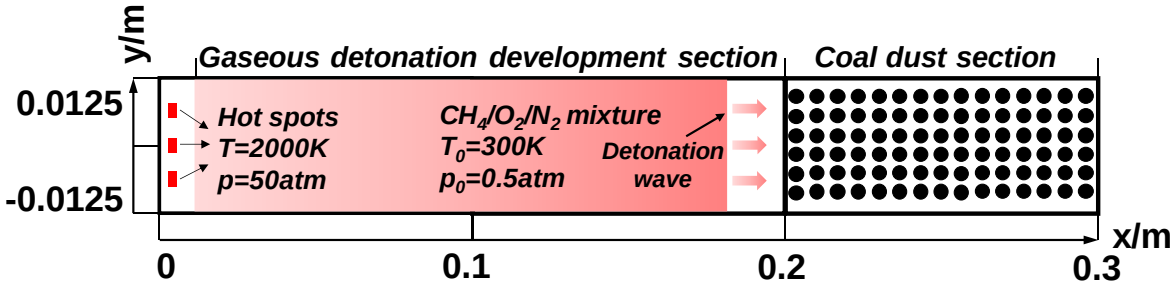


Figure 1 Schematic of the computational domain. Black dots: coal dust particles.

## 4 Results and discussion

### *4.1 Unsteady response of methane detonation to coal dust suspensions*

Figure 2 shows the peak pressure trajectory of methane detonation wave with different coal dust concentrations. They are recorded from the trajectory of maximum pressure location, normally from the triple points, when the detonation wave propagates. The result from coal-free methane detonation is also added in Fig. 2(a) for comparison. It can be observed in Fig. 2 that the presence of coal particles considerably changes the cellular structures of the detonation waves. Specifically, when the coal dust concentration is 10 g/m$^3$, the cell size is more regular, through the comparison between Figs. 2(a) and 2(b). The cell size is even smaller, in the second half of the domain ($x$ > 0.25 m), indicating more stable propagation after the coal particles are loaded.

For the coal concentration of 50 g/m$^3$ and 250 g/m$^3$ in Figs. 2(c) and 2(d), the cell size generally increases. In the latter case, the cell width is even increased to around 12.5 mm. However, when the coal concentrations are 500 g/m$^3$ and 1000 g/m$^3$ in Figs. 2(e) and 2(f), the peak pressure trajectories gradually fade when the detonation waves enter the coal area, which signifies the decoupling of the reactive front and leading shock wave and hence detonation extinction occurs. Afterwards, the detonation waves are re-initiated after the leading shock travel a finite distance (0.25 m or 0.24 m in these two cases) in the coal dust section, multiple high-pressure spots arise, leading to the re-detonation. The unsteady process will be further analyzed in Section 4.2. Further downstream, the detonation cell structures appear again, but the morphology changes considerably compared to those in other cases, i.e., in Figs. 2(b)-2(d). This indicates that higher concentrations of coal dust would inhibits the detonation wave at the initial stage, but re-detonation may occur due to the heat release of coal particle surface reactions in the shocked areas.

Figure 3 shows the evolution of the averaged leading shock propagation speed in the two-phase detonations with different coal dust concentrations. Note that these averaged results are calculated from time series of leading shock positions with a time interval of one microsecond. For comparisons, we also add the C-J speeds of particle-free $CH_4/O_2/N_2$ mixture for comparison. As demonstrated in Figs. 3(a) and 3(b), compared to the purely gaseous cases, the averaged shock speeds are generally close to the calculated C-J speed, and the speed fluctuates very little. It is seen that with increased coal dust concentration from 50 g/m$^3$ to 1000 g/m$^3$, detonation waves have a lower speed. For cases e and f,

decoupling of reactive front and shock wave occurs when the detonation wave enters the coal dust suspensions, and then re-ignites after propagating for a certain distance. Therefore, the speed of the detonation wave decreases and then increases, but the speed of case f is significantly lower after re-detonation.

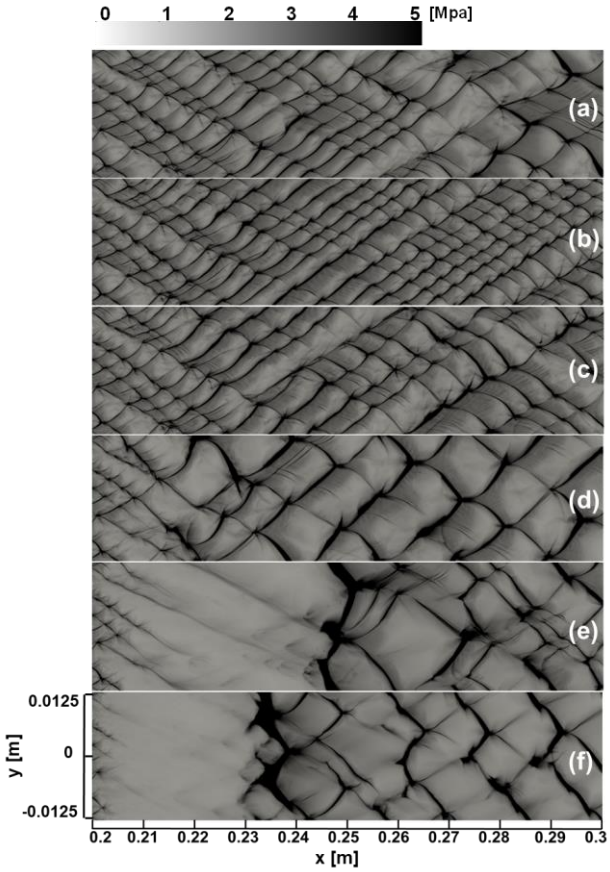


Figure 2 Peak pressure trajectory of detonation wave with different coal dust concentrations: (a) 0 g/m$^3$, (b) 10 g/m$^3$, (c) 50 g/m$^3$, (d) 250 g/m$^3$, (e) 500 g/m$^3$ and (f) 1000 g/m$^3$.

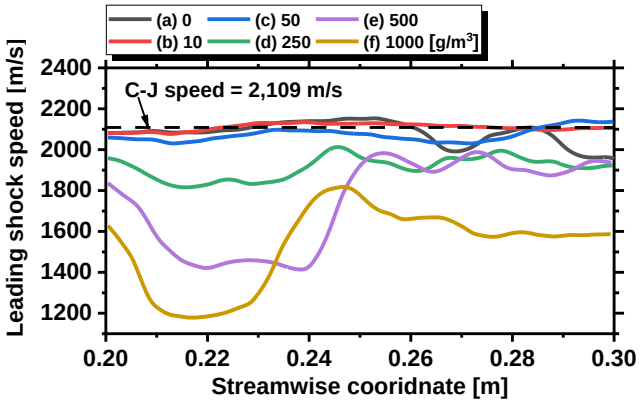


Figure 3 Evolution of average leading shock speed with various coal dust concentrations.

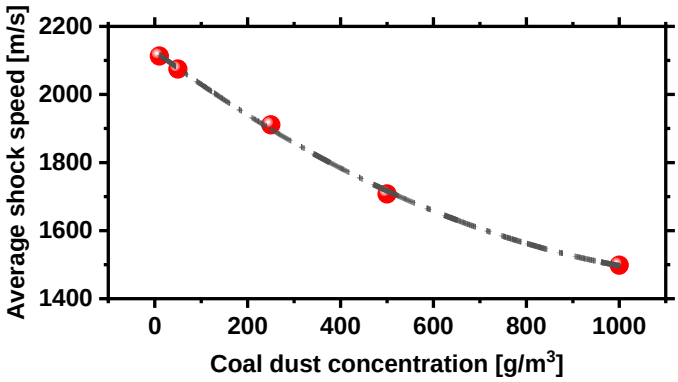


Figure 4 Change of the averaged leading shock speed as a function of coal dust concentration.

Figure 4 quantifies the variations of the averaged leading shock speed as a function of the coal dust concentrations in two-phase section (i.e., 0.2-0.3 m). It can be seen that the averaged shock speed decreases monotonically with the coal dust concentrations. This indicates that, in general, coal dust particles have an inhibitory effect on the propagation of methane detonation waves.

*4.2 Re-initiation process of methane/coal dust detonation*

For better interpretation of the methane detonation re-initiation process, the pressure gradient magnitude and heat release rate at the early stage are shown in Fig. 5(I). It is clearly seen that the high pressure point corresponds to the heat release point of the reaction front. This indicates that although the high concentration of coal dust temporarily inhibits the propagation of methane detonation, there will be high temperature and high pressure points on the two-phase reaction front, and they continue to develop and cause re-initiation.

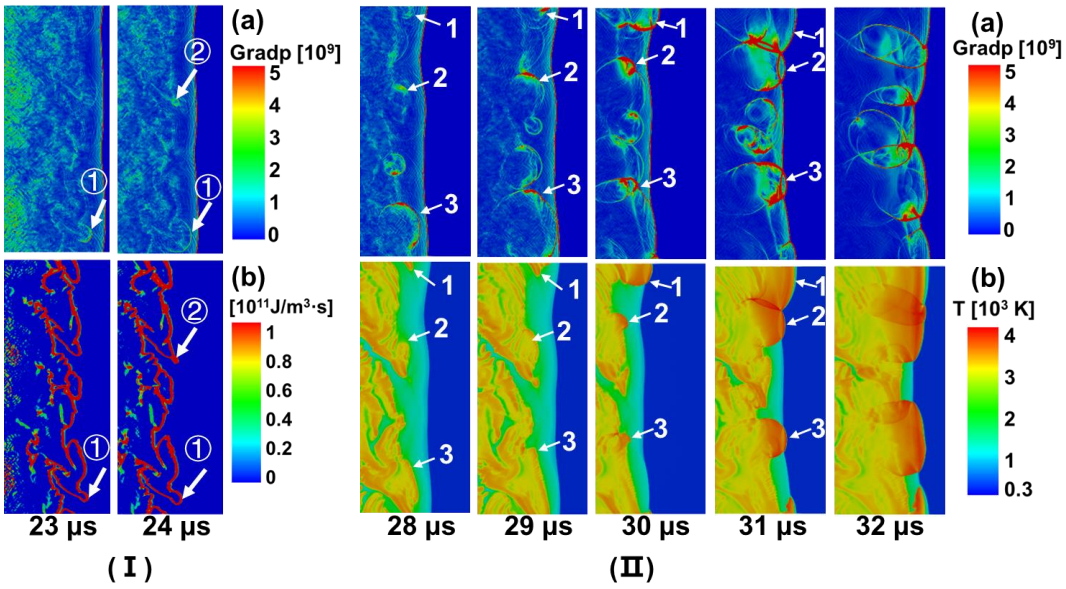


Figure 5 (I): Distributions of (a) pressure gradient magnitude and (b) heat release rate at the early stage for detonation re-initiation. ① and ②: heat release points. (II): Distributions of (a) pressure gradient magnitude and (b) gas temperature when the detonation is re-initiated. 1, 2 and 3: heat release locations. The coal dust concentrations is 1000 g/m$^3$.

The evolutions of detailed frontal structure in the foregoing re-initiation process are further illustrated in Fig. 5(II). It is found that from Fig. 5(II) at 28 μs the reaction front is fully decoupled from the leading shock front. However, one can see that from Fig. 5(II) multiple high heat release locations

(i.e., 1, 2 and 3) appear along the reaction front. These heat release points are gradually amplified as the carbon particles burn to form new shock waves. The reaction front from them gradually catches up with the leading shock wave, amd therefore detonation along the leading shock wave is intensified. Moreover, the blast waves from various chemical heat release locations collide, there by generating a high-temperature and high-pressure area (e.g., point 1 and 2 at 31 μs), which accelerates the occurrence of re-initiation.

## 5 Conclusions

Simulation of the explosions process of methane/coal dust is performed based on a two-dimensional model. The propagation process of gas and coal dust explosions under five different coal dust concentrations is analyzed. It is found that the coal dust of 10 g/m$^3$ makes the detonation wave spread more stably. However, for the coal concentration are 500 g/m$^3$ and 1000 g/m$^3$, the detonation wave appeared the phenomenon of decoupling first and then re-detonating.

## Acknowledgement

The computational work for this article was fully performed on resources of the National Supercomputing Centre, Singapore (https://www.nscc.sg/). Jingtai Shi is funded by The China Scholarship Council (202006420042).

## References

[1] A.A. Vasil Ev, A.V. Pinaev, A.A. Trubitsyn, A.Y. Grachev, A.V. Trotsyuk, P.A. Fomin, A.V. Trilis, What is burning in coal mines: Methane or coal dust? Combustion, explosion, and shock waves, 53 (2017) 8-14.
[2] M.J. Ajrash, J. Zanganeh, B. Moghtaderi, The flame deflagration of hybrid methane coal dusts in a large-scale detonation tube (LSDT), FUEL, 194 (2017) 491-502.
[3] M.J. Ajrash, J. Zanganeh, B. Moghtaderi, Methane-coal dust hybrid fuel explosion properties in a large scale cylindrical explosion chamber, J LOSS PREVENT PROC, 40 (2016) 317-328.
[4] C. Bai, G. Gong, Q. Liu, Y. Chen, G. Niu, The explosion overpressure field and flame propagation of methane/air and methane/coal dust/air mixtures, SAFETY SCI, 49 (2011) 1349-1354.
[5] Z. Huang, H. Zhang, On the interactions between a propagating shock wave and evaporating water droplets, PHYS FLUIDS, 32 (2020) 123315.
[6] Z. Huang, M. Zhao, Y. Xu, G. Li, H. Zhang, Eulerian-Lagrangian modelling of detonative combustion in two-phase gas-droplet mixtures with OpenFOAM: Validations and verifications, FUEL, 286 (2021) 119402.
[7] H. Zhang, M. Zhao, Z. Huang, Large eddy simulation of turbulent supersonic hydrogen flames with OpenFOAM, FUEL, 282 (2020) 118812.
[8] M. Zhao, Z. Ren, H. Zhang, Pulsating detonative combustion in n-heptane/air mixtures under off-stoichiometric conditions, COMBUST FLAME, 226 (2021) 285-301.
[9] M. Zhao, M.J. Cleary, H. Zhang, Combustion mode and wave multiplicity in rotating detonative combustion with separate reactant injection, COMBUST FLAME, 225 (2021) 291-304.
[10] J. Shi, Y. Xu, W. Ren, H. Zhang, Critical condition and transient evolution of methane detonation extinction by fine water droplet curtains, FUEL, 315 (2022) 123133.
[11] W. Sutherland, LII. The viscosity of gases and molecular force, The London, Edinburgh and Dublin philosophical magazine and journal of science, 36 (1893) 507-531.
[12] M.M. Baum, P.J. Street, Predicting the Combustion Behaviour of Coal Particles, COMBUST SCI TECHNOL, 3.5 (1971) 231-243.
[13] M. Stöllinger, B. Naud, D. Roekaerts, N. Beishuizen, S. Heinz, PDF modeling and simulations of pulverized coal combustion – Part 2: Application, COMBUST FLAME, 160 (2013) 396-410.
[14] X. Zhao, D.C. Haworth, Transported PDF modeling of pulverized coal jet flames, COMBUST FLAME, 161 (2014) 1866-1882.
[15] A. Kazakov, M. Frenklach, Reduced Reaction Sets Based on GRI-Mech 1.2., Available from: http://combustion.berkeley.edu/drm/drm19.dat, (1994).